AD A093289

LEVEL II

ELECTROMAGNETICS LABORATORY
TECHNICAL REPORT NO. 80-10

November 1980

WAVE TRANSMISSION THROUGH A SPHERICAL DIELECTRIC SHELL

S. W. Lee
M. S. Sheshadri
V. Jamnejad†
R. Mittra

DTIC
ELECTE
DEC 23 1980

APPROVED FOR PUBLIC RELEASE
DISTRIBUTION UNLIMITED

DDC FILE COPY

ELECTROMAGNETICS LABORATORY
DEPARTMENT OF ELECTRICAL ENGINEERING
ENGINEERING EXPERIMENT STATION
UNIVERSITY OF ILLINOIS AT URBANA-CHAMPAIGN
URBANA, ILLINOIS 61801

†JET PROPULSION LABORATORY
PASADENA, CALIFORNIA

N00019-80-C-0284
DEPARTMENT OF THE NAVY
NAVAL AIR SYSTEMS COMMAND
WASHINGTON, D.C. 20361

80 12 22 005

BLANK PAGES
IN THIS
DOCUMENT
WERE NOT
FILMED

"The views and conclusions contained in this document are those of the authors and should not be interpreted as necessarily representing the official policies, either expressed or implied, of the Naval Air Systems Command or the U.S. Government."

UNCLASSIFIED

SECURITY CLASSIFICATION OF THIS PAGE (When Data Entered)

(1) Technical rept.

REPORT DOCUMENTATION PAGE

READ INSTRUCTIONS BEFORE COMPLETING FORM

1. REPORT NUMBER	2. GOVT ACCESSION NO. AD-A093289
3. RECIPIENT'S CATALOG NUMBER	
4. TITLE (and Subtitle) WAVE TRANSMISSION THROUGH A SPHERICAL DIELECTRIC SHELL.	5. TYPE OF REPORT & PERIOD COVERED Technical
6. PERFORMING ORG. REPORT NUMBER (14) UILU	EM-80-10, UILU-ENG-80-2555
7. AUTHOR(s) (10) S. W. Lee, M. S. Sheshadri, V. Jamnejad (Jet Propulsion Laboratory), R. Mittra	8. CONTRACT OR GRANT NUMBER(s) (15) N00019-80-C-0284
9. PERFORMING ORGANIZATION NAME AND ADDRESS Department of Electrical Engineering University of Illinois Urbana, IL 61801	10. PROGRAM ELEMENT, PROJECT, TASK AREA & WORK UNIT NUMBERS RJ004
11. CONTROLLING OFFICE NAME AND ADDRESS (11) Department of the Navy Naval Air Systems Command Washington, DC 20361	12. REPORT DATE Nov 80
	13. NUMBER OF PAGES 36
14. MONITORING AGENCY NAME & ADDRESS (if different from Controlling Office) (12) 38	15. SECURITY CLASS. (of this report) UNCLASSIFIED
	15a. DECLASSIFICATION/DOWNGRADING SCHEDULE

16. DISTRIBUTION STATEMENT (of this Report)

Distribution Unlimited

APPROVED FOR PUBLIC RELEASE; DISTRIBUTION UNLIMITED

17. DISTRIBUTION STATEMENT (of the abstract entered in Block 20, if different from Report)

18. SUPPLEMENTARY NOTES

The views and conclusions contained in this document are those of the authors and should not be interpreted as necessarily representing the official policies, either expressed or implied, of the Naval Air Systems Command or the U. S. Government.

19. KEY WORDS (Continue on reverse side if necessary and identify by block number)

Antenna radome; dielectric lens; dielectric shell; ray techniques.

20. ABSTRACT (Continue on reverse side if necessary and identify by block number)

We consider the transmission of a spherical electromagnetic wave through a dielectric shell. The two surfaces of the shell are spherical (either concave or convex), and their centers are arbitrarily located in relation to the source point. The field solution determined by the geometrical optics theory is given in a simple closed form. Special attention is given to the lens effect of the dielectric shell which converts the incoming spherical pencil into a focusing pencil.

DD FORM 1 JAN 73 1473 EDITION OF 1 NOV 65 IS OBSOLETE

UNCLASSIFIED

SECURITY CLASSIFICATION OF THIS PAGE When Data Entered

408 102

UILU-ENG-80-2555

Electromagnetics Laboratory Report No. 80-10

WAVE TRANSMISSION THROUGH A SPHERICAL DIELECTRIC SHELL

Technical Report

S. W. Lee
M. S. Sheshadri
V. Jamnejad†
R. Mittra

November 1980

Department of the Navy
Naval Air Systems Command
Washington, D.C. 20361

Contract No. N00019-80-C-0284

Electromagnetics Laboratory
Department of Electrical Engineering
University of Illinois at Urbana-Champaign
Urbana, Illinois 61801

†Jet Propulsion Laboratory
Pasadena, California

APPROVED FOR PUBLIC RELEASE:
DISTRIBUTION UNLIMITED

TABLE OF CONTENTS

Accession For
NTIS GRA&I
DDC TAB
Unannounced
Justification
By
Distribution/
Availability Codes
Dist. | Avail and/or special
A

LIST OF FIGURES

I. INTRODUCTION

One of the fundamental problems in electromagnetic theory is the transmission of a spherical wave through a dielectric shell. This problem has numerous applications in antenna radomes, electromagnetic shielding, and scattering. It appears that solutions to this problem are available only for the special case where the shell is an infinite dielectric half space. That case was first studied by Sommerfeld in 1909, whereas later research was summarized in a book by Brekhovskikh (Chapter IV of [1]). In the present paper, we consider a more general case, namely, the shell has two spherical boundary surfaces. Unlike the Sommerfeld's problem, our case does include the effects of the shell's curvature and thickness. Therefore, its solution should be of more practical interest.

To solve our problem rigorously, the spherical wave expansion may be used. However, due to the fact that the source location and the two dielectric surface centers do not coincide, the translational addition theorem for vector spherical wave function [2] must be used. (Our problem is roughly comparable to scattering by three dielectric spheres.) This theorem leads to a complex series, which makes it very difficult to generate numerical results. In this paper, we use the geometrical optics theory (GO) [3], [4] to calculate the transmitted field in the problem sketched in Figure 1. Such a solution, though only approximately valid for high frequencies, is given in a simple closed form. Thus, it allows us to study the "cause and effect" of the various parameters in a convenient manner and gain physical insight.

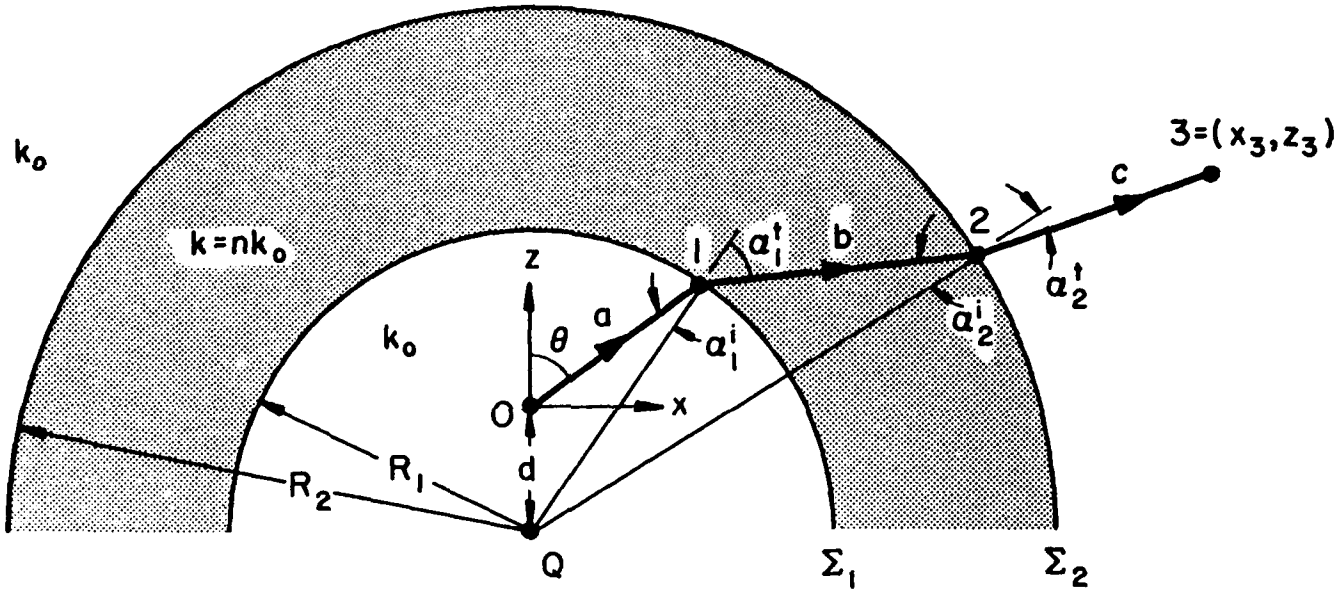

Figure 1. Transmission of a spherical wave emitted from source 0 through a spherical dielectric shell.

II. SOLUTION FOR CONCENTRIC SPHERICAL SHELL

Let us consider the wave transmission problem in Figure 1. The boundary surfaces of the dielectric shell are two concentric spheres with radii R_1 and R_2 (both positive), and with a common center at Q. The point source at 0 emits a spherical wave described by (*for exp jωt* time convention)

$$\vec{E}^i(\vec{r}) = \frac{e^{-jk_0 r}}{r} [P(\theta,\phi)\hat{\theta} + Q(\theta,\phi)\hat{\phi}] . \tag{2.1}$$

Here, (r,θ,ϕ) are spherical coordinates of $\vec{r}$ *with origin at* 0. *Functions* P and Q describe the radiation pattern of the source. The wave number $k_0 = 2\pi/\lambda_0 = \omega(\mu_0\varepsilon_0)^{1/2}$ is that of free space. By using GO [3], [4], the transmitted field at an observation point 3 is to be determined. Without loss of generality, *we assume that point* 3 lies in the (x,z)-plane with rectangular coordinates $(x_3,0,z_3)$.

A. Ray Tracing. In accordance with Snell's law, we trace a ray from source point 0 to observation point 3, via refraction points 1 and 2 (Figure 1). Clearly, all four points, 0 to 3, lie in the same (x,z)-plane. For a given launching angle θ of the ray and the distance c, the other geometrical parameters can be determined from the following relations:

$$\sin \alpha_1^i = (d/R_1)\sin \theta \quad , \quad a = R_1[\sin(\theta - \alpha_1^i)]/\sin \theta \tag{2.2}$$

$$\sin \alpha_1^t = n^{-1} \sin \alpha_1^i \quad , \quad \sin \alpha_2^i = (R_1/R_2) \sin \alpha_1^t$$

$$b = R_2[\sin(\alpha_1^t - \alpha_2^i)]/\sin \alpha_1^t \quad , \quad \sin \alpha_2^t = n \sin \alpha_2^i$$

$$x_3 = a \sin \theta + b \sin(\theta - \alpha_1^i + \alpha_1^t) + c \sin (\alpha_1^t + \alpha_2^t - \alpha_1^i - \alpha_2^i + \theta)$$

$$z_2 = a \cos\theta + b \cos(\theta - \alpha_1^i + \alpha_1^t) + c \cos(\alpha_1^t + \alpha_2^t - \alpha_1^i - \alpha_2^i + \theta) .$$

Thus, for a given (θ,c), we can determine the position of point 3 straightforwardly. On the other hand, when point 3 is given, explicit formulas do not exist for determining θ. One has to find θ by trial-and-error.

B. Field on the Ray. The present vector field problem can be decomposed into two scalar ones: one with the electric field vector perpendicular to the plane of incidence ($\vec{E} = \hat{y}\, E_\perp$) and the other with the electric field vector parallel to the plane of incidence ($E_\parallel$). The final solution for the transmitted field $\vec{E}^t$ at point 3 derived by GO is given by

$$\vec{E}^t(3) = \begin{bmatrix} E_\perp^t(3) \\ E_\parallel^t(3) \end{bmatrix} = (DF) \begin{bmatrix} T_\perp E_\perp^i(1) \\ T_\parallel E_\parallel^i(1) \end{bmatrix} e^{-jk_0(nb+c)} . \tag{2.3}$$

The various factors in (2.3) are explained below: $T_\perp$ and $T_\parallel$ are the products of the transmission coefficients at points 1 and 2, given by

$$T_\perp = 4\left[1 + n\frac{\cos\alpha_1^t}{\cos\alpha_1^i}\right]^{-1}\left[1 + \frac{1}{n}\frac{\cos\alpha_2^t}{\cos\alpha_2^i}\right]^{-1} \tag{2.4a}$$

$$T_\parallel = 4\left[1 + \frac{1}{n}\frac{\cos\alpha_1^t}{\cos\alpha_1^i}\right]^{-1}\left[1 + n\frac{\cos\alpha_2^t}{\cos\alpha_2^i}\right]^{-1} . \tag{2.4b}$$

The two components of the incident field are calculated from (2.1):

$$E_\perp^i(1) = \frac{e^{-jk_0a}}{a} Q(\theta,\phi = 0) \tag{2.5a}$$

$$E_\parallel^i(1) = \frac{e^{-jk_0a}}{a} P(\theta,\phi = 0) . \tag{2.5b}$$

The derivation of the divergence factor DF in (2.3) requires some effort. With the details given in Appendix A, the final result for DF reads

$$DF = (1 + \kappa_{11}b)^{-1/2} (1 + \kappa_{12}b)^{-1/2} (1 + \kappa_{21}c)^{-1/2} (1 + \kappa_{22}c)^{-1/2} . \quad (2.6)$$

At point 1 or 2, it can be shown that the principal directions of the transmitted wavefront are precisely the two directions parallel and perpendicular to the plane of incidence. Here $(\kappa_{11},\kappa_{12})$ are the two principal curvatures of the transmitted wavefront at point 1, and $(\kappa_{21},\kappa_{22})$ are those at point 2. They are calculated from the relations

$$\kappa_{11} = (n \cos^2 \alpha_1^t)^{-1}\left[\frac{1}{a} \cos^2 \alpha_1^i + \frac{1}{R_1}(n \cos \alpha_1^t - \cos \alpha_1^i)\right] \quad (2.7a)$$

$$\kappa_{12} = \frac{1}{na} + \frac{1}{R_1}(\cos \alpha_1^t - \frac{1}{n} \cos \alpha_1^i) \quad (2.7b)$$

$$\kappa_{21} = (\cos^2 \alpha_2^t)^{-1} \left[(b + \kappa_{11}^{-1})^{-1} n \cos^2 \alpha_2^i + \frac{1}{R_2}(\cos \alpha_2^t - n \cos \alpha_2^i)\right] \quad (2.7c)$$

$$\kappa_{22} = n(b + \kappa_{12}^{-1})^{-1} + \frac{1}{R_2}(\cos \alpha_2^t - n \cos \alpha_2^i) . \quad (2.7d)$$

The sign convention of κ is as follows. If κ is positive (negative), the normal section of the wavefront is divergent (convergent). For example, if the transmitted wavefront at point 1 is the same as the incident spherical wavefront, we have $\kappa_{11} = \kappa_{12} = +R_1^{-1}$. For a typical factor in (2.6), the square root convention is

$$f = (1 + \kappa b)^{-1/2} = \begin{cases} +|f|, & \text{if } f \text{ is real} \\ +j|f|, & \text{if } f \text{ is imaginary} \end{cases} \quad (2.8)$$

When f is imaginary, it means that the ray has crossed a focus of the ray pencil. The (+j) accounts for the well-known $(\pi/2)$ phase retardation.

Several general comments about the solution in (2.3) are in order: (i) For the case where a total reflection occurs (α_1^t or α_2^t becomes complex), the field in the transmitted region is not an optical field, and the present ray solution (2.3) is no longer valid. (ii) Except for special cases, e.g., normal incidence $\alpha_1^i = 0$, the two curvatures (κ_{21},κ_{22}) of the transmitted wavefront emerging from the dielectric shell are not equal. Thus, the transmitted pencil is generally astigmatic. (iii) It is possible that κ_{21} and/or κ_{22} are negative. Then the divergent pencil from the source is transformed into a convergent (focusing) pencil after propagating through the dielectric shell. (iv) The solution in (2.3) remains valid for more geometries than the one shown in Figure 1. This is discussed further in the next section.

III. GENERALIZATION OF FINAL SOLUTION

For transmission through the concentric spherical shell in Figure 1, the final solution consists of two parts:

Part A: Ray tracing formulas in (2.2)

Part B: Field solution in (2.3) through (2.5)

It can be shown that Part B is valid under a more general condition (Figure 2), namely,

(i) The centers of the spherical shells Q_1 and Q_2 need not coincide, as long as the four points (0,1,2,3) are coplanar.

(ii) The surfaces of the shell can be either concave or convex. Looking from the source side, R_1 (or R_2) is positive if the surface is concave, and R_1 is negative if the surface is convex.

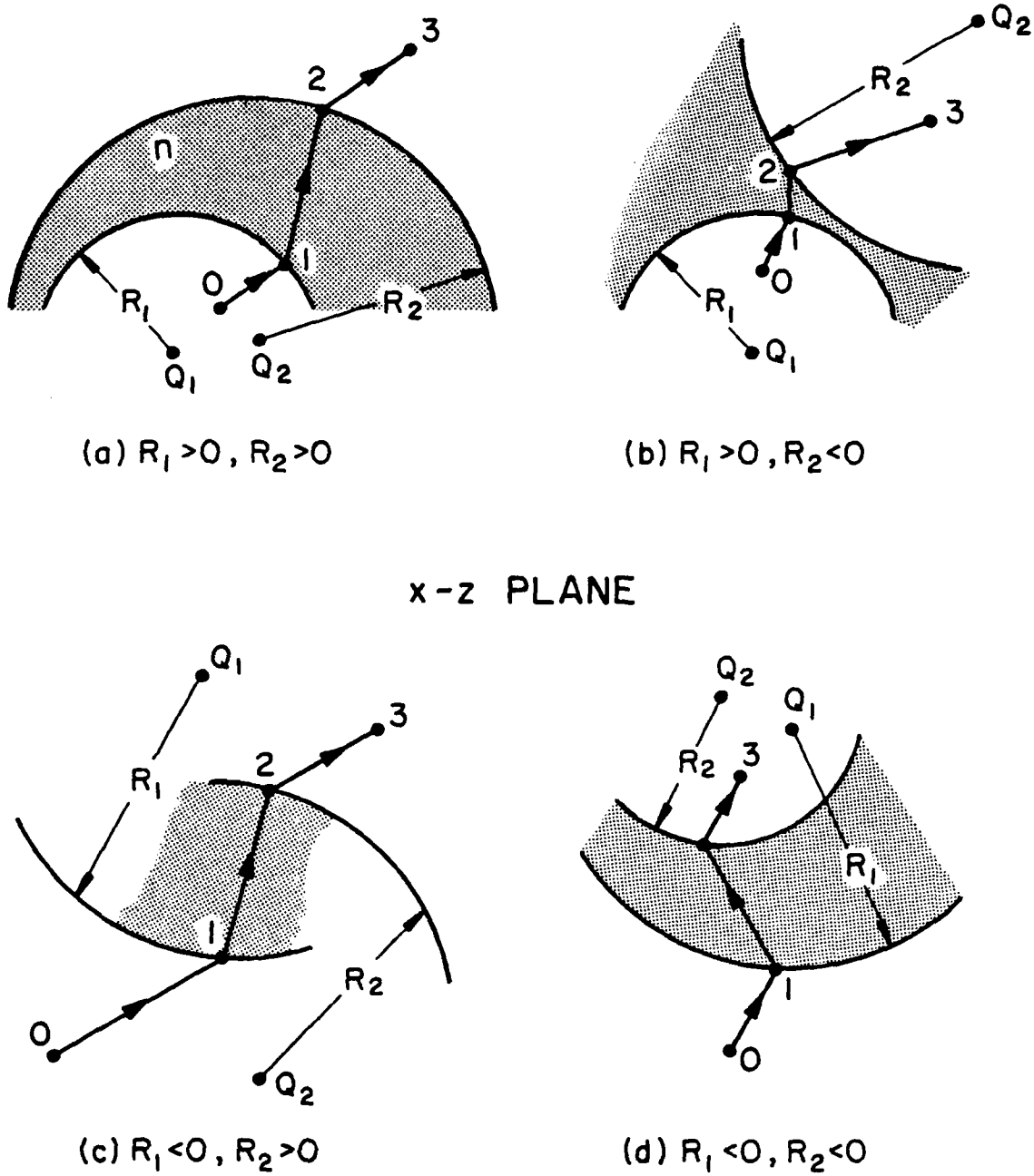

Figure 2. General configurations where the field solution (2.3) can be used. Points (0,1,2,3) must be coplanar.

Condition (i) is necessary in order for the scalar transmission coefficients $T_\perp$ and $T_{||}$ in (2.4) to be valid. When the four points (0,1,2,3) are not coplanar, the perpendicular and parallel polarizations are no longer uncoupled. Then the scalar $T_\perp$ or $T_{||}$ in (2.3) must be replaced by a (2 × 2) matrix. Also, (2.7) becomes more complicated.

For the general configurations in Figure 2, the ray tracing formulas in (2.2) are not valid. However, by following Snell's law, the ray tracing even in the most general situation is conceptually simple. Thus, instead of working out a set of general formulas, we leave it to the individual problems.

IV. AXIAL INCIDENCE ON SYMMETRICAL SHELLS

To study the features of the present ray solution, let us concentrate on a special case, where the four points $(Q_1,Q_2,0,3)$ are on a straight line (Figure 3). Then the four curvatures in (2.7) reduce to

$$\kappa_{11} = \kappa_{12} = \frac{1}{na} + \frac{n-1}{n\,R_1} \tag{4.1a}$$

$$\kappa_{22} = \kappa_{21} = \frac{nR_1 + an(n-1)}{bR_1 + ab(n-1) + na\,R_1} + \frac{1-n}{R_2} = \frac{n}{b + \kappa_{11}^{-1}} + \frac{1-n}{R_2} \tag{4.1b}$$

An interesting question is "When does κ_{11} or κ_{22} become negative (meaning a convergent circle)?" This is answered below:

(i) Negative κ_{11}. The transmitted pencil inside the dielectric shell is a convergent one when $\kappa_{11} < 0$ or

$$a > \left(\frac{1}{1-n}\,R_1\right) > 0 \tag{4.2}$$

If $R_1 > 0$ (concave dielectric interface shown in Figure 4a), this is possible if $n < 1$. If $R_1 < 0$ (convex dielectric interface shown in Figure 4b),

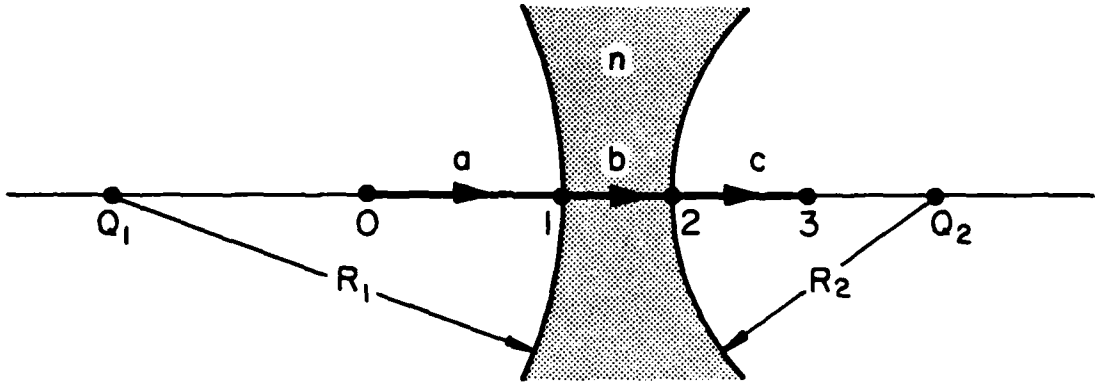

Figure 3. Axial incidence on a symmetrical shell. In this example, $R_1 > 0$ (concave) and $R_2 < 0$ (convex).

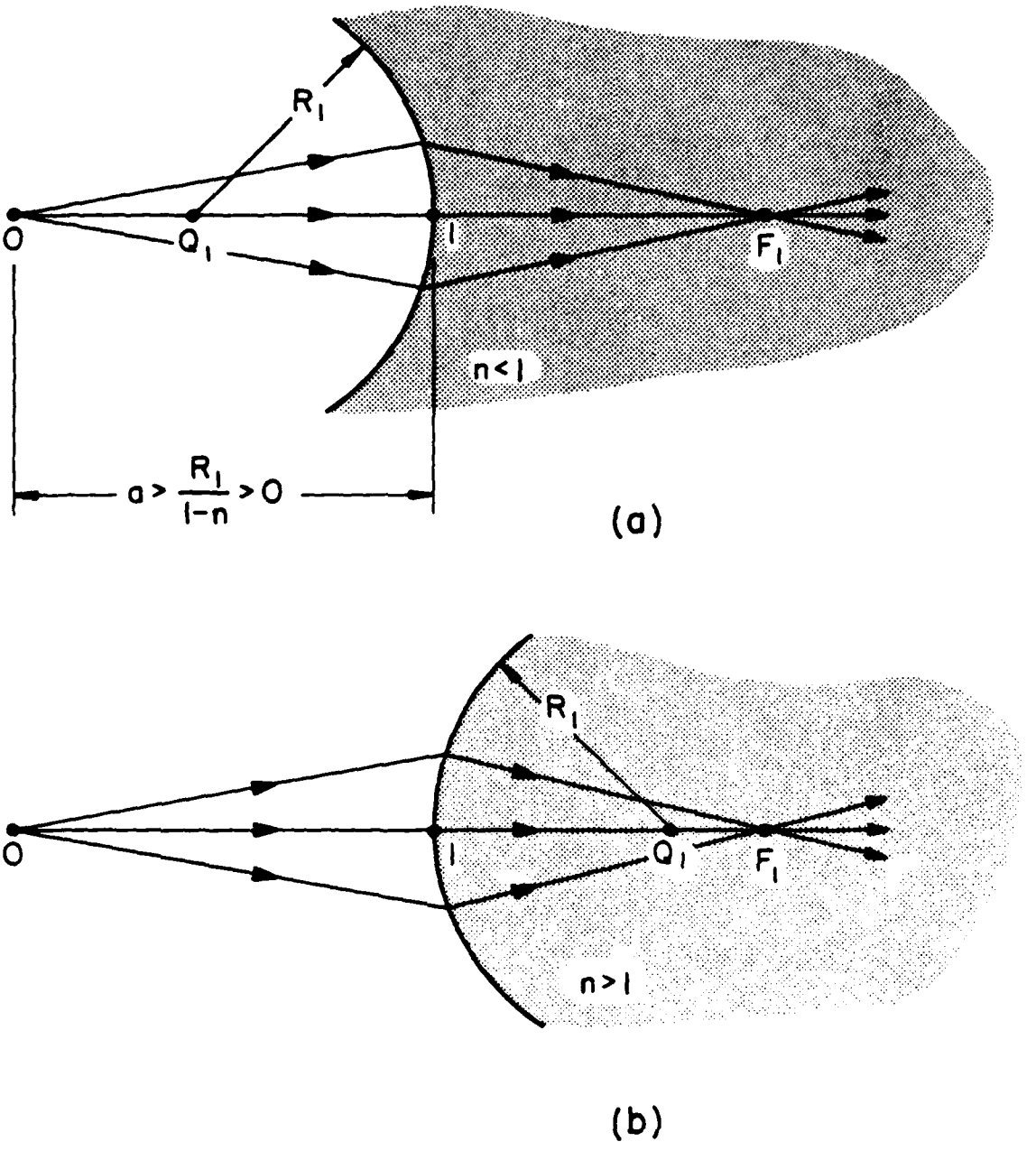

Figure 4. Condition for a convergent beam inside the dielectric shell. (a) Concave interface. (b) Convex interface.

this is possible only if n > 1. The distance between point 1 and focal point F_1 is $(\kappa_{11})^{-1}$.

(ii) Negative κ_{22}. The transmitted field in the free-space region outside the dielectric shell is convergent when $\kappa_{22} < 0$. Let us concentrate on a special case in which the thickness of the dielectric shell is small so that

$$b << \kappa_{11}^{-1} \cdot \tag{4.3}$$

Then κ_{22} in (4.1b) becomes approximately

$$\kappa_{22} \simeq \frac{1}{a} + (n - 1)\left(\frac{1}{R_1} - \frac{1}{R_2}\right) \cdot \tag{4.4}$$

which is the well-known equation for the thin lens. (See for example Eq. (41-1), p. 685 of [5]. Note the corresponding notations used in [5] and here: $s = -a$, $s' = -\kappa_{22}^{-1}$, $R_1 = -R_1$, and $R_2 = -R_2$.) The condition for a negative κ_{22} under the approximation in (4.3) is

$$a > \frac{R_1 R_2}{(n - 1)(R_1 - R_2)} > 0 \cdot \tag{4.5}$$

(iii) Far Field: If the observation point 3 is in the far zone ($\kappa_{22} c >> 1$), then DF in (2.6) becomes

$$DF \sim \left\{\frac{a}{a + \frac{1}{n} b + c}\right\} \left\{1 + (n - 1) \frac{ab}{R_1 R_2} \left[\frac{R_2 - R_1}{b} \sim 1 + \frac{1}{n}\left[1 - \frac{R_1}{a}\right]\right]\right\}^{-1} \cdot \tag{4.6}$$

The first factor in { } in (4.6) is the divergence factor of a planar dielectric slab ($R_1, R_2 \to \infty$). Thus, the ratio of the electric field at a far-field point 3 for a spherical shell and that for a dielectric slab is

$$\eta = \frac{|\vec{E}^t(3) \text{ for spherical shell}|}{|\vec{E}^t(3) \text{ for a slab of same thickness}|}$$

$$= \left\{1 + (n-1)\frac{ab}{R_1R_2}\left[\frac{R_2 - R_1}{b} - 1 + \frac{1}{n}\left(1 - \frac{R_1}{a}\right)\right]\right\}^{-1} . \qquad (4.7)$$

As a numerical example, consider the case in which the inner and outer dielectric surfaces are concave and concentric ($Q_1 = Q_2$) with $(R_1/b) = 2$. We plot η as a function of (a/b) for $n = 0.5$ and $n = 3$ in Figure 5. We note that η can be substantially different from unity. When $a = R_1$, we have $\eta = 1$. Thus, in this interesting special case, the axial far field through a concentric spherical shell and that through a planar slab become the same. Another interesting special case occurs when $DF \to \infty$. It means that the paraxial rays emerging from the dielectric shell (Figure 3) are parallel to the axis so that they focus at the far-field point at infinity. From (4.6), it is shown that $DF \to \infty$ if $\kappa_{22} = 0$ or

$$\frac{1}{a} = (n-1)\frac{R_1 - R_2 + b(n-1)/n}{R_1[R_2 - b(n-1)/n]} . \qquad (4.8)$$

Under the thin-lens approximation $b \simeq 0$, (4.8) is reduced to the well-known lensmaker's equation (see Eq. (41-2), p. 685 of [5]). In the antenna radome application, (4.8) is useful in the determination of the enhancement of the antenna main beam.

(iv) Multiple Refraction: For a given source point 0 and observation point 3 in Figure 1 or 2, we can trace two types of geometrical optics rays. The first type is the direct ray from 0 to 3 without going through internal reflections in the dielectric shell. Its field solution is given in (2.3) which, of course, is the main contribution. The second type contains rays which bounce one or more times inside the shell before reaching point 3. We now consider the contribution of such multiply refracted rays. For the

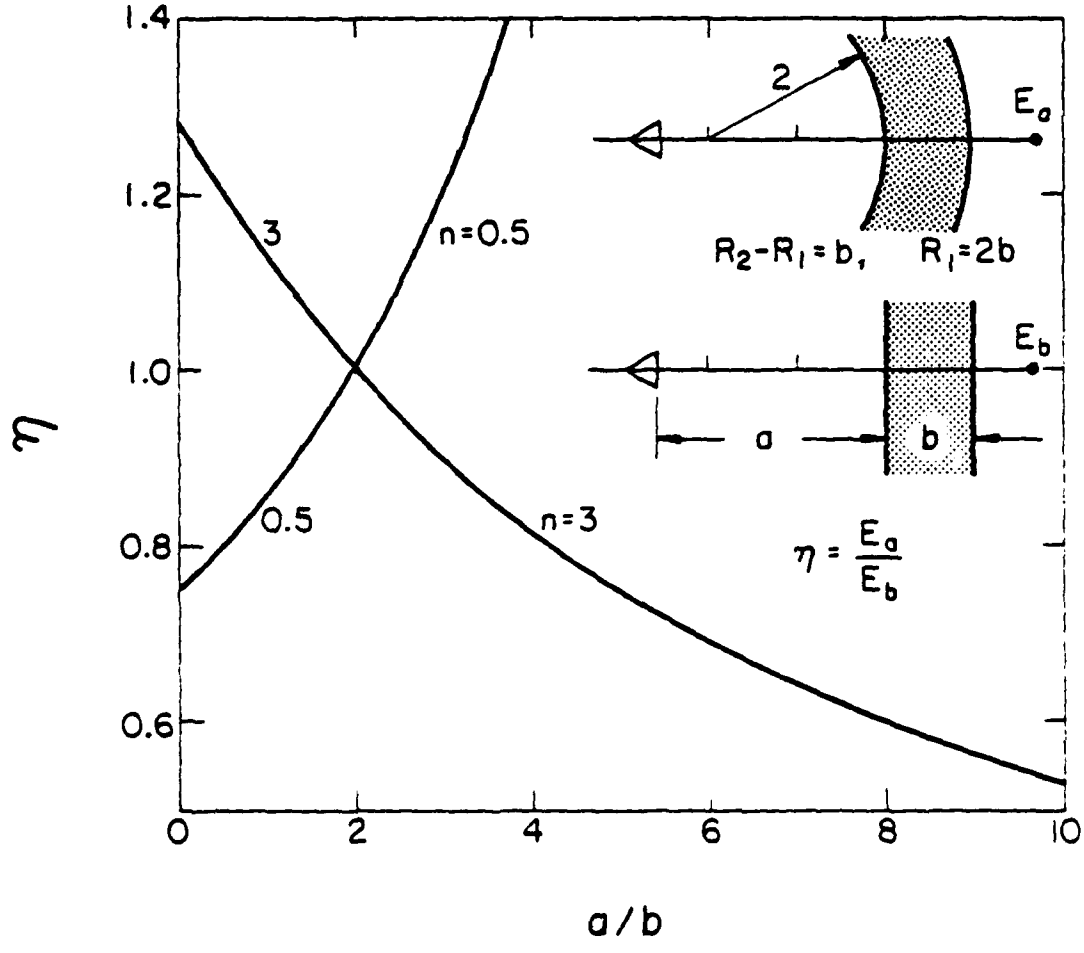

Figure 5. Transmitted field E_a transmitted through a spherical shell normalized by E_b which is that through a dielectric slab.

axial incidence case (Figure 3), let us further specialize the geometry by setting $(R_1, R_2) \to \infty$. The dielectric shell becomes the slab shown in Figure 6, and the field on the direct ray calculated from (2.3) reads

$$\vec{E}^t(3) = \vec{E}^i(1)\, e^{-jk_0(nb+c)} \left[\frac{a}{na + b + nc}\right] T \tag{4.9}$$

where T is the product of the transmission coefficients at points 1 and 2 (Figure 6a)

$$T = T_1 T_2 = \left[\frac{2}{1 + n}\right]\left[\frac{2}{1 + (1/n)}\right] . \tag{4.10}$$

In a similar manner, we can calculate the field on the multiply refracted rays (a twice internally refracted ray is shown in Figure 6b). Superimposing their contributions, we obtain the solution for the field at point 3 including the direct and <u>all</u> multiply refracted rays, namely,

$$[\vec{E}^t(3)]_{\text{all rays}} = \vec{E}^i(1)\, e^{-jk_0(nb+c)} \left[\frac{na}{na + b + nc}\right] T \cdot \left\{1 + \sum_{p=1}^{\infty} e^{-j2pk_0 nb} \left(\frac{n - 1}{n + 1}\right)^{2p} \frac{na + b + nc}{na + (2p + 1)b + nc}\right\} . \tag{4.11}$$

Under the condition

$$(a + c) \to \infty \text{ (far field), or } b \to 0 \text{ (thin slab)} \tag{4.12a}$$

the series in (4.11) can be summed up in a closed form with the result

$$[E^t(3)]_{\text{all rays}} = \vec{E}^i(1)\, e^{-jk_0(nb+c)} \left[\frac{na}{na + b + nc}\right] T_{\text{slab}} \tag{4.12b}$$

when T_{slab} is recognized as the transmission coefficient of the slab

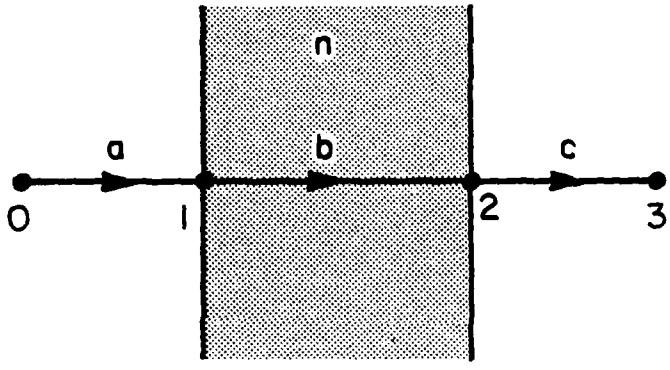

(a)

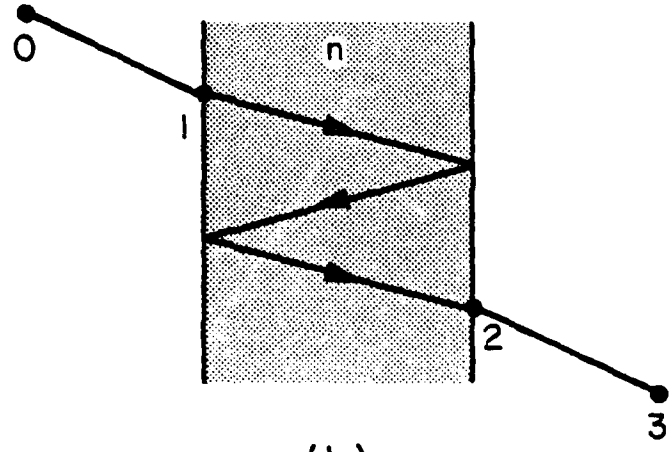

(b)

Figure 6. Singly and doubly refracted rays through a dielectric slab.

$$T_{slab} = \frac{T}{1 - \left(\frac{n-1}{n+1}\right)^2 \exp(-j2k_0 nb)} \quad . \tag{4.12c}$$

Comparing (4.12b) with (4.9), we note the effect of the multiply refracted rays is accounted for by replacing T by T_{slab}. When the condition in (4.12a) is not met, we must evaluate (4.11) numerically. Let us define an error term

$$\delta_p = \left\{ \frac{|\vec{E}^t(3)| \text{ including p multiply refracted rays}}{|\vec{E}^t(3)| \text{ including all multiply refracted rays}} - 1 \right\} \times 100\% \quad . \tag{4.13}$$

In Figure 7, we plot δ_0 (including no multiply refracted rays) and δ_1 (including one multiply refracted ray) vs. n for $b = 0.75\ \lambda_0$ and $(a + c)/b = 4$. Several observations are made. (a) For commonly used values of n (between 1 and 3), the error δ_0 is 13% or less except at resonances. A resonance occurs when all multiply refracted rays emerging from the slab are in phase with the primary ray. For the configuration in Figure 6, the resonance condition is

$$(nk_0 b/\pi) = (2nb/\lambda_0) = \text{a positive integer} \quad . \tag{4.14}$$

For an obliquely incident ray and/or a curved slab, the condition for resonance is rarely satisfied. Thus, generally speaking, the error for neglecting the multiple refraction is roughly 10%. (b) Errors δ_0 and δ_1 have about the same order of magnitude. Thus, the inclusion of the first-order multiply refracted ray does not in general improve the accuracy of the solution.

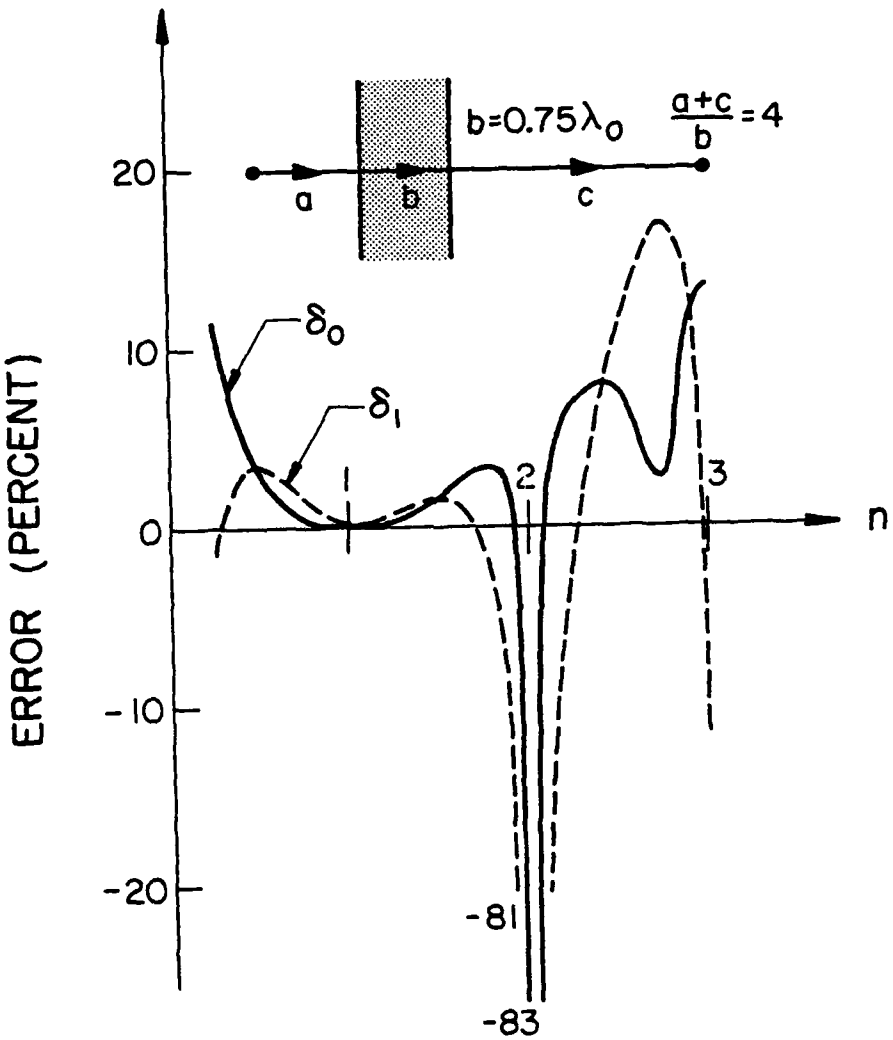

Figure 7. Error introduced by neglecting all or all except one multiply refracted ray in a dielectric slab.

V. NUMERICAL RESULTS

A. Radome. Consider a dielectric spherical radome with an inner radius 20 λ_0, a uniform thickness 0.5 λ_0 and n = $\sqrt{5}$, as shown in Figure 8. The y-polarized source is located at points 1, 3, or 4, and its radiation field in the E-plane is given by

$$\vec{E}^i(r,\theta,\phi = \pi/2) = \frac{e^{-jk_0 r}}{r} [\hat{y} \cos (1.5\ \theta)] \quad . \tag{5.1}$$

The transmitted field is calculated from (2.3). For an observation point in the E-plane and in the far-field zone (x = 0 plane and c → ∞ in Figure 1), we may rewrite (2.3) as

$$\vec{E}^t(\vec{r}) \sim \frac{e^{-jk_0 r}}{r} [\hat{y}\ p^t(\theta)] \quad , \quad r \to \infty \tag{5.2}$$

where r is the distance from point 0 to point 3 (Figure 1). We plot $p^t(\theta)$ as a function of θ in Figure 8. Generally speaking, the radome modifies the radiation field gently, as expected.

B. Lens I (Double Concave). Unlike the above radome, a dielectric lens may modify the incident field drastically. Let us consider Lens I, drawn approximately to scale in Figure 9. The source is 2 λ_0 away from the lens, and is y-polarized. Let us concentrate on the field in the H-plane (x-z plane). In Figure 9, we launch 4 rays 2° apart. The outside ray (at θ = 6°) suffers total reflection at the second face of the lens, and is not transmitted into the free space region (we ignore multiple refractions). We assume the incident field from the source is confined to a cone (a beam). In the x-z plane, it is given by

$$\vec{E}^i(x,0,z) = \frac{e^{-jk_0 r}}{r} \begin{cases} \hat{y}\ 1 & , \quad \text{if} \quad \theta < \theta^i \\ 0 & , \quad \text{if} \quad \theta > \theta^i \end{cases} . \tag{5.3}$$

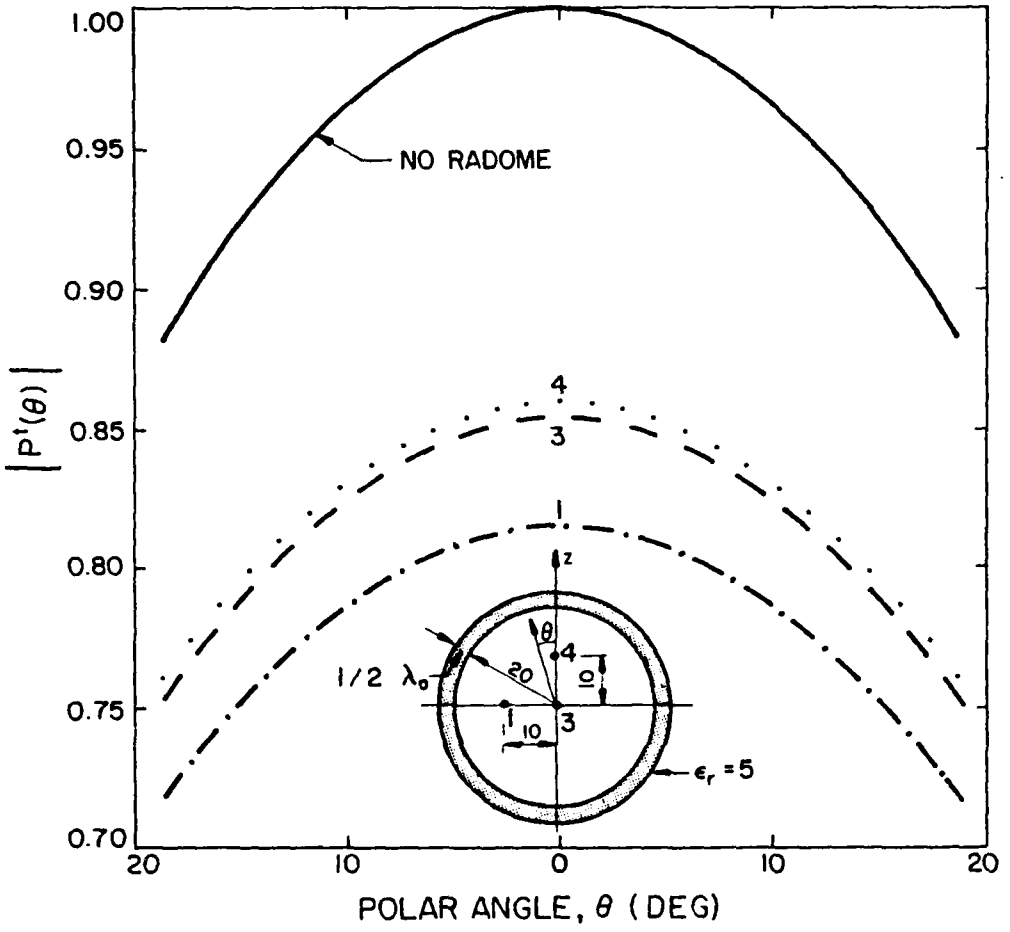

Figure 8. E-plane radiation pattern through a spherical radome.

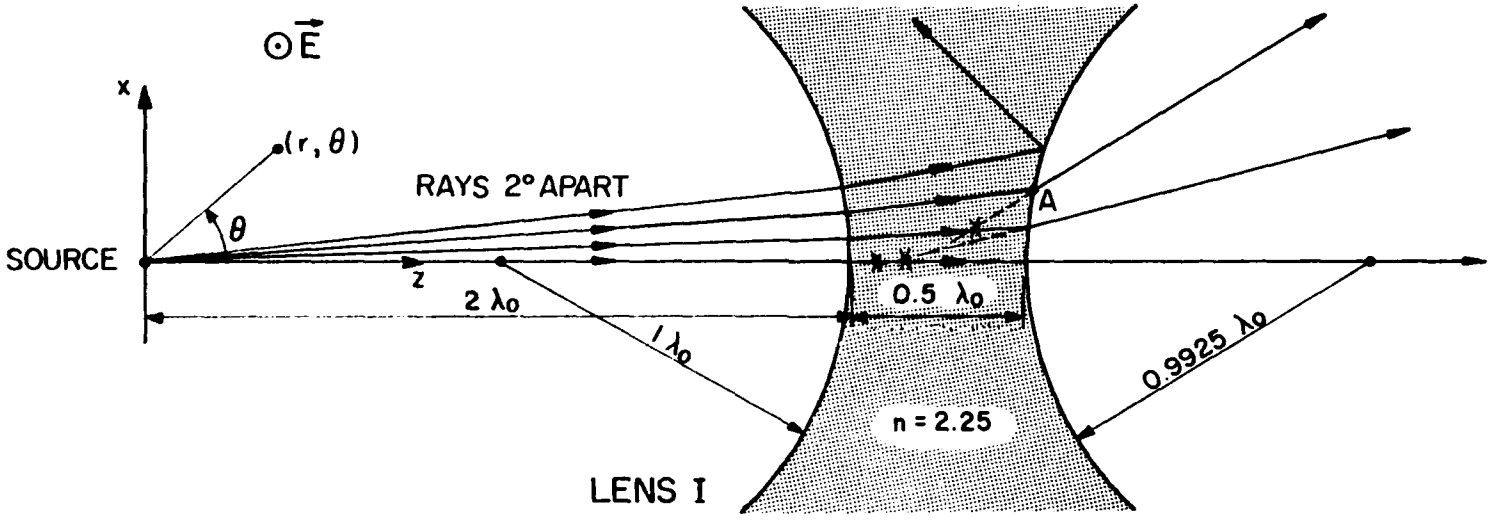

Figure 9. Double-concave spherical dielectric lens: geometry and ray picture. Crosses indicate foci.

In the present case (Lens I), we choose $\theta^i = 5.5°$. After transmission through the lens, the rays become more divergent, and they are spread over an angular region of about $\theta < 53.5°$, which is considerably wider than the incident angular spread ($\theta < 5.5°$). At an observation point $(r,\theta,\phi = 0)$, we express the transmitted field as

$$\vec{E}^t(r,\theta,0) = \frac{e^{-jk_0 r}}{r} [\hat{y}\, Q^t(r,\theta)] \quad . \tag{5.4}$$

In the absence of the lens, $Q^t = 1$ for $\theta < \theta^i$ and $Q^t = 0$ for $\theta > \theta^i$. With the lens present, we plot $Q^t(r,\theta)$ as a function of θ for $r = 2 \times 10^3\ \lambda_0$ in Figure 10. Note that the transmitted field is much weaker (12% or less) than the incident field because of the wider spread of the transmitted rays. For the present case, $Q^t(r,\theta)$ is only very weakly dependent on r, as long as $r > 100\ \lambda_0$. Thus, the transmitted field $\vec{E}^t$ in (5.4) in the far zone is approximately a spherical wave with an angular pattern Q^t. Every transmitted ray has two foci. Their distance behind the second face Σ_2 of the lens is $(\kappa_{21})^{-1}$, and $(\kappa_{22})^{-1}$, which may be calculated from (2.7). In particular, $(\kappa_{21})^{-1}$ is for the normal section of the wavefront in the plane of incidence (x-z plane), whereas $(\kappa_{22})^{-1}$ is for that in the perpendicular plane (defined by the y-axis and the ray direction). For the third ray (incident $\theta = 4°$) in Figure 9, we calculate from (2.7) that

$$(\kappa_{21})^{-1} = +0.21\ \lambda_0 \quad , \quad (\kappa_{22})^{-1} = +0.375\ \lambda_0. \tag{5.5}$$

We mark the position of the focus corresponding to κ_{21} by a cross in Figure 9. The distance between A and the cross is $(\kappa_{21})^{-1}$. The trace of the two sets of foci is shown in Figure 11. They are curves on the two caustic surfaces of the transmitted wavefront (intersection of caustic surfaces and the x-z plane).

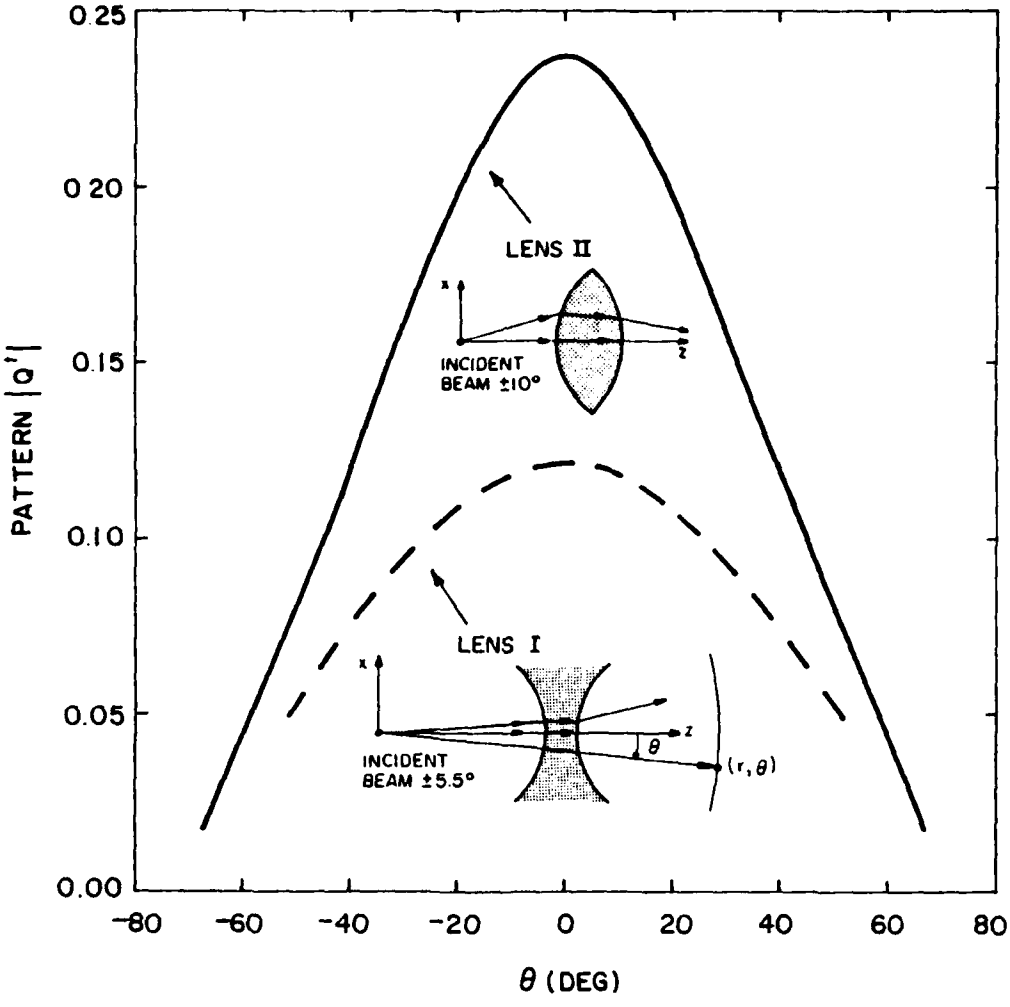

Figure 10. H-plane far field pattern through lens I and lens II.

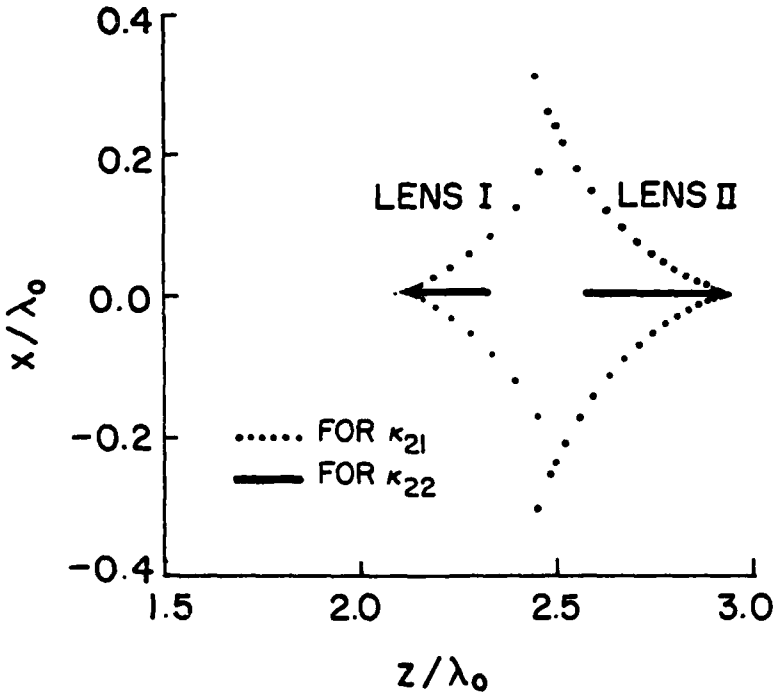

Figure 11. Trace of foci of the transmitted rays which lie in x-z plane for lenses I and II. (For better presentation, the scale along the x-axis is expanded.)

C. Lens II (Double Convex). The geometry of Lens II and its ray picture are shown in Figure 12. The incident field is given in (5.3) with $\theta^i = 10°$. The transmitted field in the H-plane is expressed in (5.4), where $Q^t(r,\theta)$ is again very weakly dependent on r in the far zone and is plotted in Figure 10. We note that the incident 10°-beam is now spread into a 67°-beam after transmission through Lens II. The peak value of the transmitted field is about 24% of the incident field at the same far-field location. The caustic curves are shown in Figure 11.

D. Lens III (Convexo-Concave). The geometry of Lens III is shown in Figure 13. The radii (R_1,R_2) of the lens and the source distance satisfy the lensmaker's equation in (4.8), so that the transmitted rays near the axial direction are almost parallel and focus at a point at infinity in the axial direction. The incident field is given in (5.3) with $\theta^i = 12°$. The H-plane transmitted field $\vec{E}^t$ is expressed in (5.4), where $Q^t(r,\theta)$ varies drastically from the near field zone up to $r \sim 100\ \lambda_0$ as seen from Figure 14. Beyond $r \sim 100\ \lambda_0$, the beam becomes narrower, and the peak becomes higher with the increase of r. It is well-known that the exact value of the beam's peak (on a caustic surface) cannot be predicted by the present geometrical optics theory. It can be calculated from, for e.g., the Huygens-Green formula described in p. 107 of [7]. The caustic curves are shown in Figure 15.

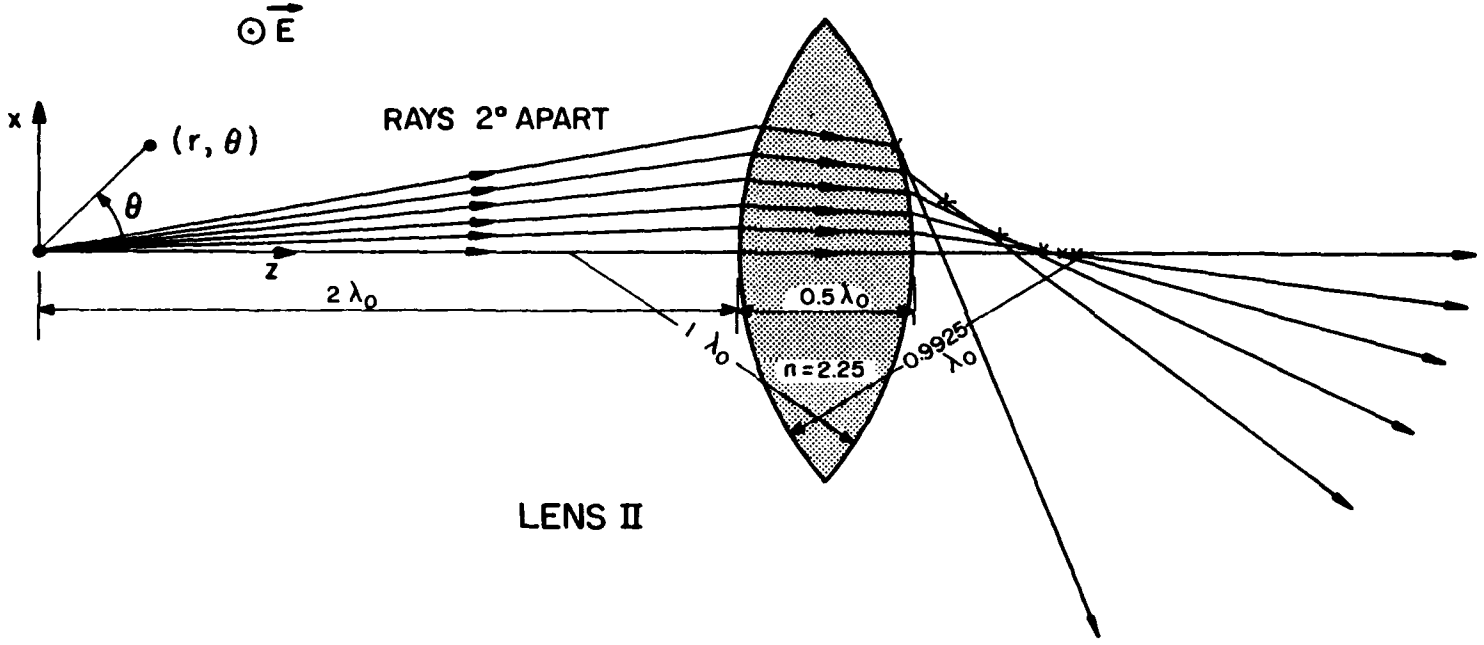

Figure 12. Double-convex spherical dielectric lens: geometry and ray picture. Crosses indicate foci.

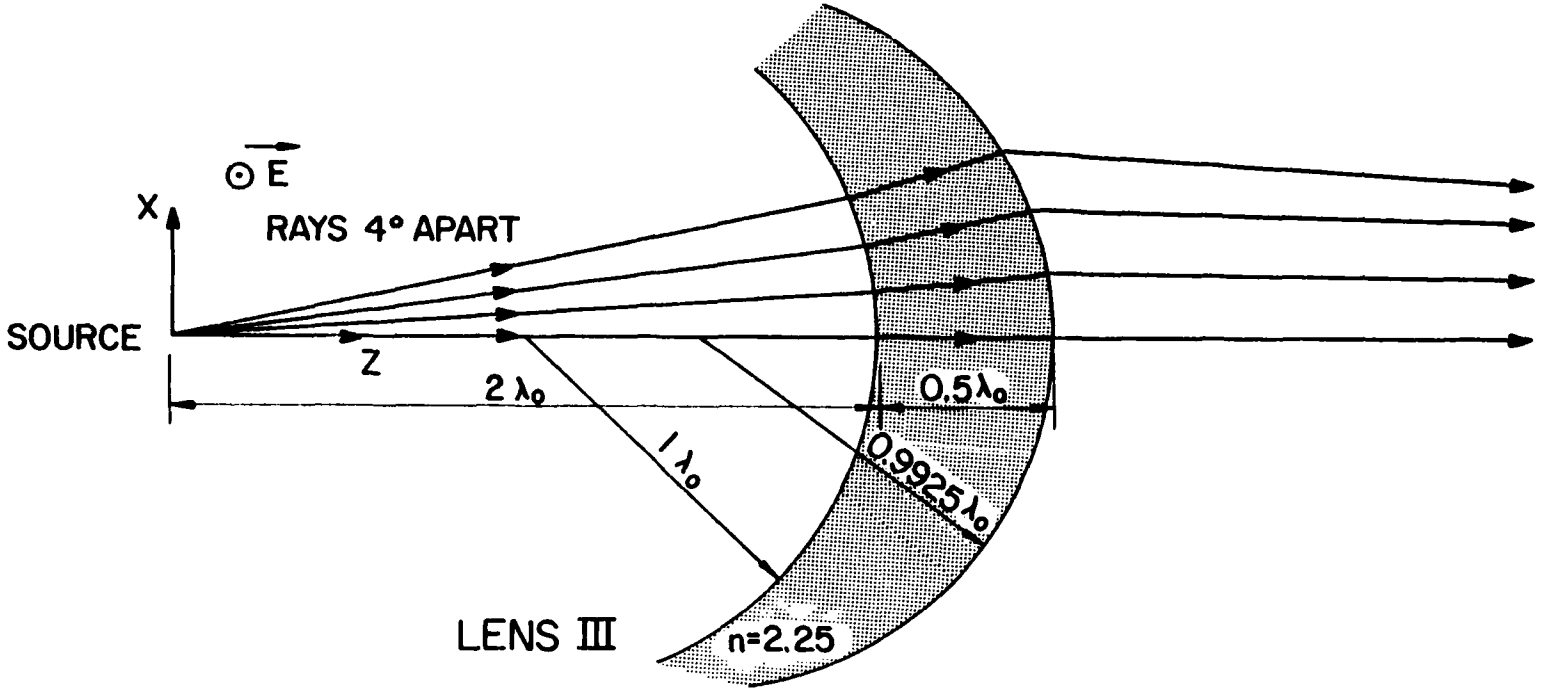

Figure 13. Convexo-concave spherical dielectric lens: geometry and ray picture.

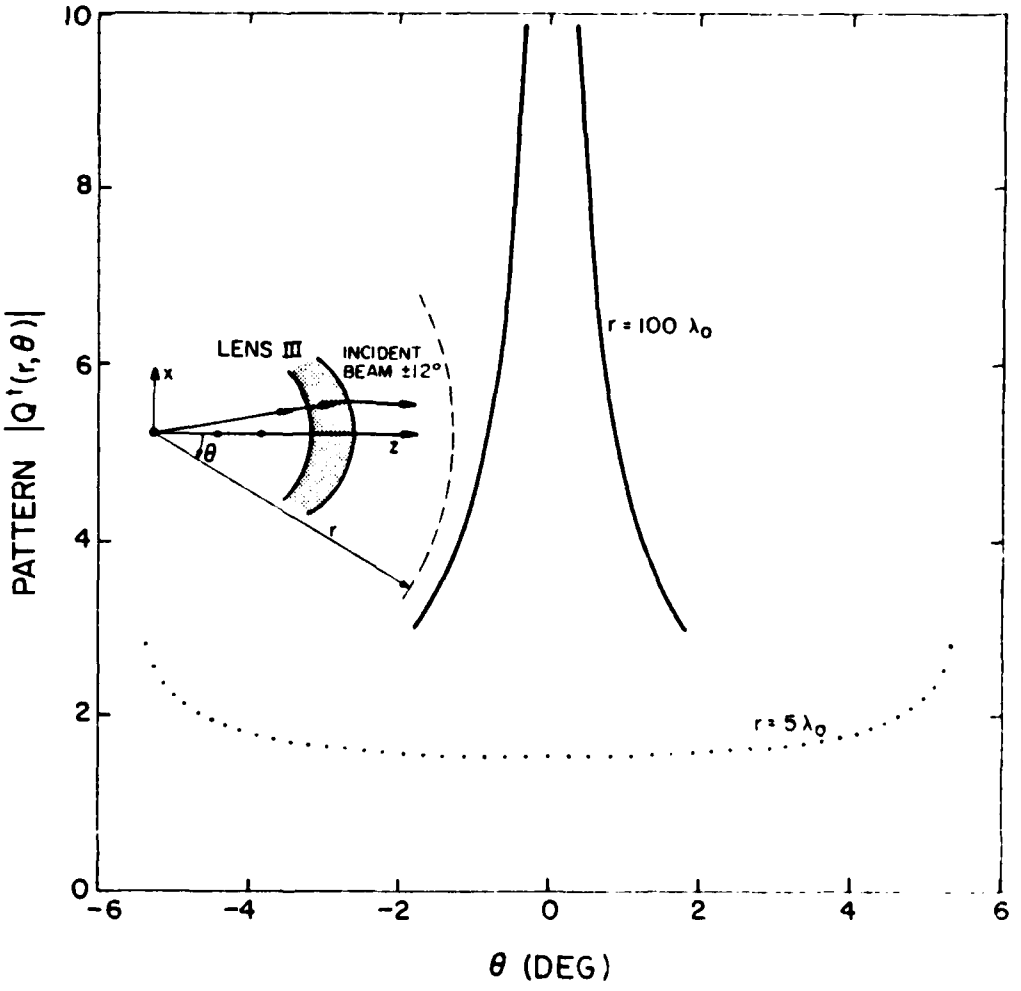

Figure 14. H-plane far field pattern through lens III.

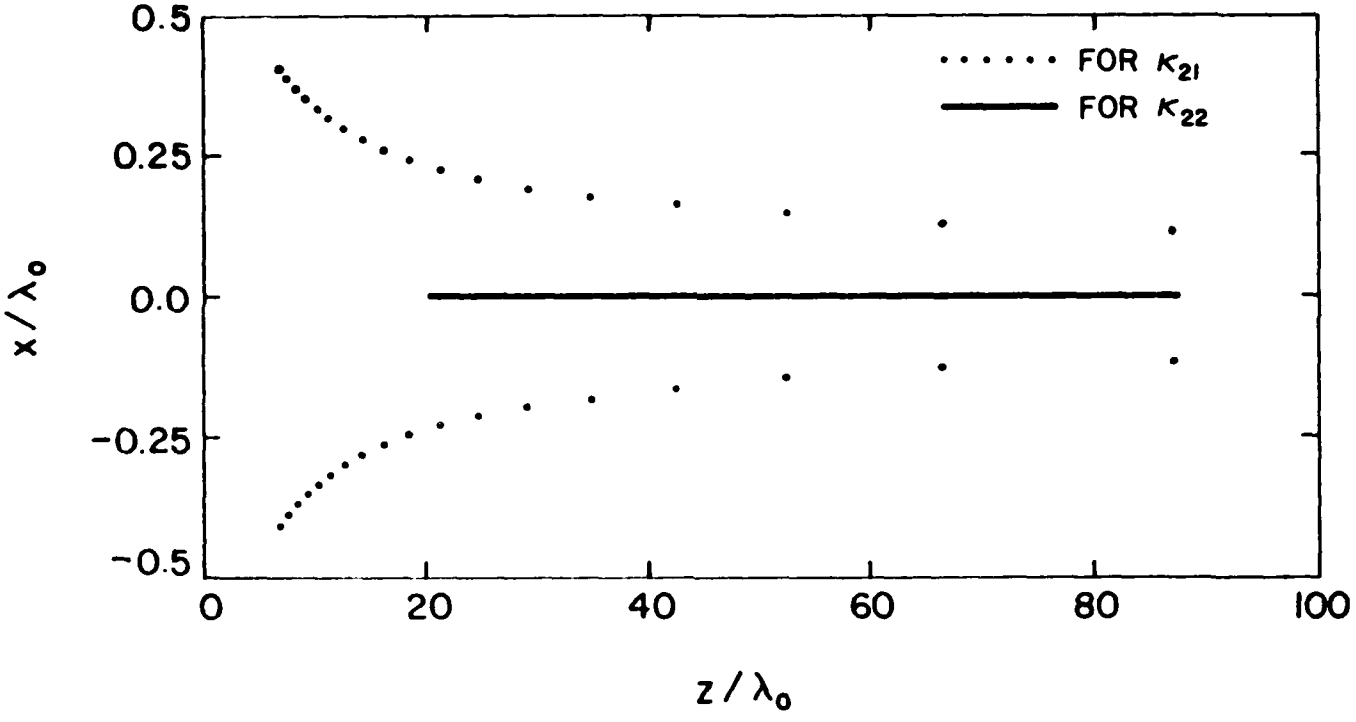

Figure 15. Trace of foci of the transmitted rays which lie in the x-z plane, for lens III.

VI. CONCLUSION

For a given incident field in (2.1), a geometrical optics solution of the transmitted field through a spherical dielectric shell (Figure 2) is given in (2.3) through (2.7). The present solution is approximately valid when (i) the source frequency is high (the radii of curvature of the curved shell are large in terms of wavelength), (ii) the four points (0,1,2,3) in Figure 2 are coplanar, and (iii) the observation point is away from the caustic surfaces of the transmitted wavefront. Furthermore, our solution includes only the contribution from the first-order refracted ray (a direct ray from the source to the observation point without internal refractions inside the dielectric shell). It has been estimated that, except at "resonances" which rarely occur for curved shells, the error of neglecting higher-order refracted rays is roughly 10% for $n = \sqrt{\epsilon_r}$ in the range 1 to 3.

REFERENCES

[1] L. M. Brekhovskikh, Waves in Layered Media. New York: Academic Press Inc., 1960.

[2] J. H. Bruning and Y. T. Lo, "Multiple scattering of EM waves by spheres: Part I - Multipole expansion and ray-optical solutions; Part II - Numerical and experimental results," IEEE Trans. Antennas Propagat., vol. AP-19, no. 3, pp. 378-400, May 1971.

[3] G. A. Deschamps, "Ray techniques in electromagnetics," Proc. IEEE, vol. 60, no. 9, pp. 1022-1035, Sept. 1972.

[4] S. W. Lee, P. Cramer, Jr., K. Woo and Y. Rahmat-Samii, "Diffraction by an arbitrary subreflector: GTD solution," IEEE Trans. Antennas Propagat., vol. AP-27, no. 3, pp. 305-316, May 1979.

[5] F. W. Sears, M. W. Zemansky, and H. D. Young, University Physics, 5th ed. Massachusetts: Addison-Wesley, 1976.

[6] S. W. Lee, "Differential geometry for GTD applications," Technical Report EM 77-21, University of Illinois, Urbana, IL, 1977.

[7] S. Silver, Microwave Antenna Theory and Design. New York: Dover, 1965.

APPENDIX A

DERIVATION OF EQUATION (2.6)

Referring to Figure 1, the curvature matrix [3], [6] of the incident spherical wave may be expressed as

$$Q_1^i = \begin{bmatrix} a^{-1} & 0 \\ 0 & a^{-1} \end{bmatrix} \tag{A.1}$$

The curvature matrix of the inner surface of the radome (Σ_1) is

$$Q^{\Sigma_1} = \begin{bmatrix} R_1^{-1} & 0 \\ 0 & R_1^{-1} \end{bmatrix} \tag{A.2}$$

From the knowledge of these two curvature matrices, the curvature matrix of the refracted ray 1-2 may be expressed as [3]

$$Q_1^t = (\theta_1^t)^{-1}[\theta_1^i Q_1^i \theta_1^i/n + (\cos \alpha_1^t - \cos \alpha_1^i/n)Q^{\Sigma_1}](\theta_1^t)^{-1} \tag{A.3}$$

where θ_1^i and θ_1^t are coordinate transformation matrices given by

$$\theta_1^i = \begin{bmatrix} \cos \alpha_1^i & 0 \\ 0 & 1 \end{bmatrix} \tag{A.4}$$

$$\theta_1^t = \begin{bmatrix} \cos \alpha_1^t & 0 \\ 0 & 1 \end{bmatrix} \tag{A.5}$$

Simplifying (A.3), we obtain

$$Q_1^t = \begin{bmatrix} \kappa_{11} & 0 \\ 0 & \kappa_{12} \end{bmatrix} \tag{A.6}$$

where κ_{11} and κ_{12} are defined in (2.7).

The curvature matrix of the wavefront incident at point 2 is given by

$$Q_2^i = [(Q_1^t)^{-1} + b\,\bar{\bar{I}}]^{-1} \tag{A.7}$$

where $\bar{\bar{I}}$ is the identity matrix. The curvature matrix of the transmitted wavefront at 2 can be calculated similarly to that at 1. The final result is

$$Q_2^t = \begin{bmatrix} \kappa_{21} & 0 \\ 0 & \kappa_{22} \end{bmatrix} \tag{A.8}$$

where κ_{21} and κ_{22} are defined in (2.7).